In Proceedings of the 2nd Joint Meeting of the US Sections of the Combustion Institute, Oakland, March 25-28, 2001.

Three-Dimensional Flame Propagation Above Liquid Fuel Pools *

Jinsheng Cai, Feng Liu, and William A. Sirignano

Department of Mechanical and Aerospace Engineering
University of California, Irvine, CA 92697-3975

Ignition and flame spread above liquid fuels initially below the flashpoint temperature are studied. Opposed air flow to the flame spread due to forced and/or natural convection is considered. Unsteady computations are performed in order to study the ignition event and to describe both uniform and pulsating flame spread. Pools of finite width and length are studied in air channels of prescribed height and width, thereby requiring a three-dimensional space resolution in order to capture the effects at the edge of the pool and at the side walls of the air channel. The effects of variations in surface tension due to surface temperature variations and of buoyancy in both the liquid and gas phases are considered. One-step chemical kinetics, Fickian diffusion, Fourier heat conduction, and laminar flow with variable properties are considered. Boundary layers at the walls and at the liquid/gas interface are resolved. A moving mesh scheme is employed to follow the flame motion. Regions of pulsation are found at both 1-g and 0-g. Average flame speed and pulsation frequency increase with initial fuel temperature. Surface tension can have a major effect, e.g., cause a recirculation. Buoyancy can modify flame speed and flame shape. The flame extends over the edge of the pool producing some clearly three-dimensional effects such as lateral air motion. The computations are intended to guide and to explain experiments that are being performed at NASA Glenn by H. Ross and F. Miller.

1 Introduction

Schiller, Ross, and Sirignano [1] studied ignition and flame spread above liquid fuels initially below the flashpoint temperature by using a two-dimensional computational fluid dynamics code that solves the coupled equations of both the gas and the liquid phases. Their computational studies and analysis identified the mechanisms for uniform and pulsating flame spread and studied the effects of gravity level, pool depth, fluid properties, and chemical kinetic coefficients on flame spread across liquid fuel pools. Pulsating flame spread was attributed to the establishment of a gas-phase recirculation cell that forms just ahead of the flame leading edge because of the opposing effect of buoyancy-driven flow in the gas phase and the thermocapillary-driven flow in the liquid phase. Schiller and Sirignano [2] extended the same study to include flame spread with forced opposed flow in the gas phase. A transition flow velocity was found above which an originally uniform spreading flame becomes pulsating. The same type of gas-phase recirculation cell caused by the combination of forced opposed flow, buoyancy-driven flow, and thermocapillary-driven concurrent flow was found to be responsible for the pulsating flame spread. Ross and Miller [3] and Miller and Ross [4] performed experimental work that corroborate the computational findings in References 1 and 2.

In this paper, we extend previous two-dimensional and axisymmetric studies in References 1, 2, and 5 to three-dimensions. Pools of finite width and length are studied in air channels of prescribed height and width, thereby requiring a three-dimensional space resolution in order to capture the effects at the edge of the pool and at the side walls of the air channel. The effects of variations in surface tension due to surface temperature variations and of buoyancy in both the liquid and gas phases are considered. One-step chemical kinetics, Fickian diffusion, Fourier heat conduction, and laminar flow with variable properties are considered. Boundary layers at the walls and at the liquid/gas interface are resolved. Unsteady computations are performed in order to study the ignition and flame spreading event. As in the two-dimensional case, both pulsating and uniform spread have been observed. The computations, however, capture that the effects of the fuel-tray-edge that cause a curvature of the flame in the spanwise direction. Preliminary results show that the three-dimensional code will be a useful tool to ultimately guide and to explain experiments that are being performed at NASA Glenn by H. Ross and F. Miller. See, for example, References 3 and 4.

*Paper presented at the 2nd Joint Meeting of the US Sections of the Combustion Institute, Oakland, March 25-28, 2001.

2 Physical Description of the Problem

Figure 1 shows the geometry of the three-dimensional model. A shallow pool of liquid n-propanol fuel is placed in a rectangular wind tunnel. The liquid pool surface is made flush to the wind tunnel floor to simplify the computation. Initially, the liquid and the air in the tunnel are assumed to be at the same temperature T_0. On start of computation, air is forced to blow over the liquid fuel. Computation without reaction is performed for 1 second to establish the boundary layer and fuel vapor profiles in the gas phase before the igniter shown in Figure 1 is activated. The igniter is modelled as a hot pocket of gas with a temperature that increases linearly from T_0 to 1700 K in 0.01 s. The igniter temperature is kept constant until the flame has travelled 1 cm, after which the igniter is turned off.

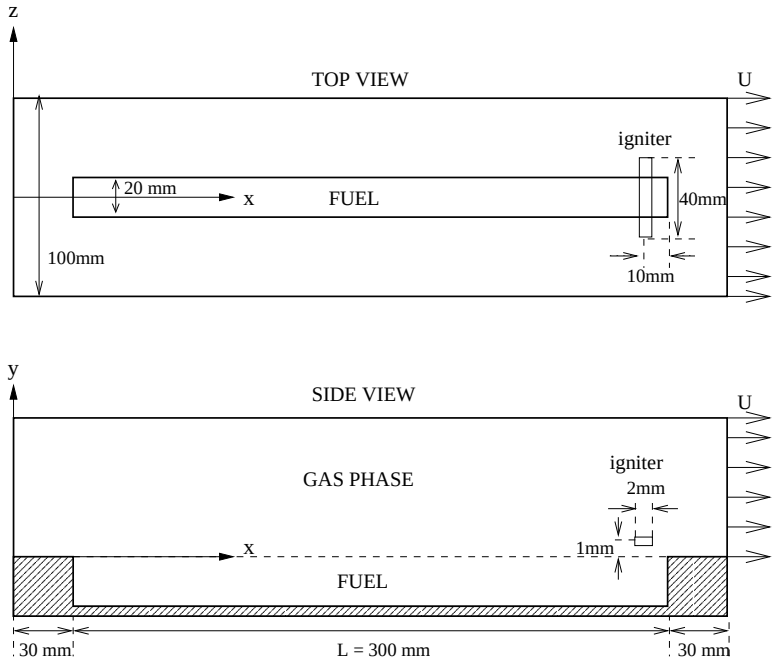

Figure 1: Geometry for the three-dimensional liquid fuel pool in a wind-tunnel with forced flow

3 Assumptions and Boundary Conditions

The mathematical formulation of the problem and the assumptions are the same as those in References 2 but are now extended to three dimensions. The boundary conditions at the gas/liquid interface follow from a heat balance and balance of the shear stresses with surface tension; a continuity of the temperature and tangential velocity; no dissolution of air or combustion products into the liquid; and negligible recession of the liquid surface. The fuel vapor concentration at the liquid surface is assumed to be $X_F = P_{sat}(T)/P_a$, where $P_a = 1$ atm is the ambient pressure. Temperature gradients along the liquid surface create thermocapillary stresses in the following balance: $(\mu\frac{\partial u}{\partial y})_l = \mu(\frac{\partial u}{\partial y})_g + \sigma_T(\frac{dT}{dx})_{lg}$ in the x direction and $(\mu\frac{\partial w}{\partial y})_l = \mu(\frac{\partial w}{\partial y})_g + \sigma_T(\frac{dT}{dz})_{lg}$ in the z direction. In general, the stresses due to the surface tension is several orders of magnitude larger than the viscous stresses in the gases phase except for some isolated points. Therefore, the latter may be neglected in the computation.

Zero normal gradient boundary conditions are used in the gas phase at the tunnel inlet while a uniform flow of velocity U is applied at the exit of the tunnel. No slip boundary conditions are applied on the wind tunnel walls. Adiabatic boundary conditions are used on all wind tunnel and liquid pool walls.

4 Numerical Method

The numerical method uses the SIMPLE algorithm [6] modified to use an approximate factorization method to perform sub-iterations within each implicit time step. Only half of the wind tunnel is considered due to symmetry. A non-uniform mesh of $62 \times 42 \times 36$ in the gas phase with clustered grid points in the flame region is used. The mesh for the liquid phase has 20 grid points in depth and coincides with the mesh in the gas phase over the liquid surface. The grid lines in the streamwise direction and along the width of the tunnel are redistributed to concentrate in the flame region every time the flame front has moved 1 mm. Linear interpolation is used to map each dependent variable from the old to the new grid.

5 Results and Discussion

Six cases as listed in Table 1 are studied that correspond to the initial temperatures $T_0 = 15°C$,$19°C$, and $21°C$, and at normal gravity and zero gravity. The geometry of the fuel pool is shown in Figure 1. The depth of the fuel pool is fixed at 2 mm and air is assume to contain 21% oxygen by volume for the results presented in this paper. The flow velocity at the exit of the wind tunnel is fixed at 30 cm/s for all four cases. Notice that the flow velocity at the inlet of the wind tunnel will then vary with time and is slightly lower than 30 cm/s due to gas expansion after ignition.

Initial Temperature	**Normal Gravity (1 g)**	**Zero Gravity (0 g)**
$\mathbf{T_0 = 21°C}$	Case 1A	Case 1B
$\mathbf{T_0 = 19°C}$	Case 2A	Case 2B
$\mathbf{T_0 = 15°C}$	Case 3A	Case 3B

Table 1: Cases Studied in this paper.

Figure 2 shows the calculated history of flame fronts for all six cases versus time. The position of the flame front is determined by the x position of the maximum fuel consumption rate in the flow field at each time instant. The x values decrease as the flames move upstream. Figure 2 clearly shows that the flames with higher initial fuel and air temperatures propagate faster than those at lower initial temperatures. For the same initial temperatures, the flames at normal gravity move faster than those at zero gravity due to the fact that buoyancy increases the entrainment of air and fuel vapor into the flame region. Figure 2 also shows that the flame front exhibits pulsating motion for all conditions considered. The pulsating frequency increases as the initial air and fuel temperature increases. It is expected that the flame may propagate steadily with a uniform speed at higher temperatures than what is currently investigated in this paper. On the other hand, gravity effects increase the pulsating frequency as well as the mean flame speed. Figures 3 and 4 plot the mean flame speeds and periods of pulsation frequencies for the six cases that are estimated by using the data shown in Figure 2.

In the rest of this paper, the details of the flame structure are examined for the two cases 1A and 1B for $21°C$ under normal and microgravity, respectively. These results from the two cases present a qualitative description of the other four cases as well.

Case 1A. Figure 2 indicates that the flame is propagating in the fast mode at $t = 1.63$ seconds after ignition for this case. At this time instant, Figure 5 shows the contours of fuel consumption rate in the x-y symmetry plane of the fuel pool ($z/L = 0.0$). The highest reaction zone clings close to the fuel pool with two tails curving upwards in the back. Figure 6 shows contours of the temperature and flow velocity vectors in the same x-y plane. In the laboratory reference frame, both surface tension of the liquid fuel and thermal expansion appear to cause the fluid move forward ahead of the flame. However, a plot of the relative flow velocities observed when moving with the flame shown in Figure 7 reveals that a thin layer of premixed fuel-air mixture ahead of the flame is fed into the flame near the liquid surface. The existence of this layer accounts for the high intensity of the combustion.

Figure 8 plots the flow velocity U_{lg}, fuel vapor vertical velocity V_{lg}, temperature T_{lg} on the fuel-air interface, and the maximum fuel consumption rate (searched in the y direction) at each x location through the flame region.

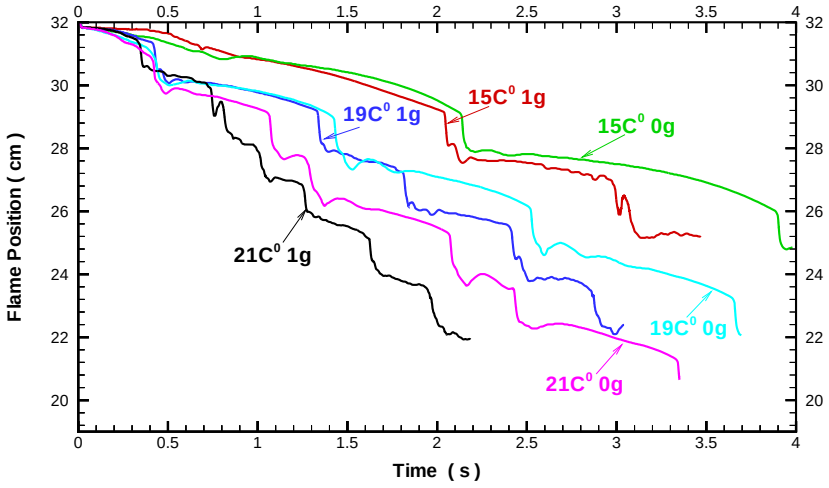

Figure 2: Flame location versus time after ignition.

The maximum fuel consumption ratio indicates that the flame is very thin. Temperature rises sharply through the thin flame and then stays high behind the flame. Fuel vaporizes the fastest below the flame front but continues to vaporize behind the flame. Surface tension causes the flow to move upstream because of the strong temperature negative gradient in that direction.

Figure 9 shows a top view of the flame in terms of the contours of fuel consumption rate at $y = 1$ mm distance from the pool surface. The edge of the fuel pool is marked by the dashed line. Apparently, the strongest reaction is at the moving flame front on the left. The flame curves around at the edge of pool and trails along the edge downstream, forming a diffusion flame held by the pool edge. Part of the flame extends over the pool edge, especially near the corner of the flame front, where there is the largest relative diffusion surface area. The reaction near that region is , however, slower compared to that in other parts of the flame. Notice, also, that the flame bifurcates into two branches at the corner similar to that at the flame front in the side view shown in Figure 5. The 'pilot' branch is a premixed flame due to the fact that the fuel pool is allowed to vaporize and diffuse into the air stream before ignition.

In order to see the flame structure along the pool edge, the flow field is examined at two cross sections normal to the free stream at $x/L = 0.691$ and 0.788, respectively. Figure 10 shows the fuel consumption rate in the first cross section, which cuts through the moving flame front. The pool edge is indicated by the dashed line in the figure. The flame extends significantly beyond the pool edge over the floor of the wind tunnel although it is still dominated by the strong reaction zone in the main flame front. Figure 11 shows the temperature contours and velocity vectors in the same cross plane. Thermal expansion pushes the flow away from the flame zone. On the pool surface side, however, surface tension pulls the fluid towards the center of the pool where the fluid is cooler. This lateral motion initiates a streamwise vortex along the pool edge.

The second cross section is some distance behind the moving flame front at $x/L = 0.788$. Figures 12 and 13 show the contours of the fuel consumption rate, and the velocity vectors and temperature contours in this section. At this downstream station, the main flame front disappears and we are left with a lateral flame attached to the pool edge. The streamwise vortex initiated at the earlier cross section is now amplified, being assisted by both surface tension in the pool and buoyancy effect that draws air into the flame from the fuel pool. This is clearly seen in the velocity field shown in Figure 13.

The flame continues to propagate at relatively high speed until it slows down significantly at $t = 1.7$ second. At $t = 1.87$ second, the flame is almost stagnant. Figure 14 shows the contours of the fuel consumption rate and Figure 15 shows the relative velocity vectors and the temperature distribution at this instant. Since the flame is almost stagnant at this instant, the relative and absolute velocity fields are similar. Unlike at time $t = 1.63$ second when the flame is moving fast, thermal variation of the surface tension pulls the fluid ahead of the flame front while the opposing air flow and buoyancy effect cause the flow to move in the opposite direction. This causes a clockwise vortex cell in front of the flame as shown by the relative velocity vectors in Figure 15. Unlike in the

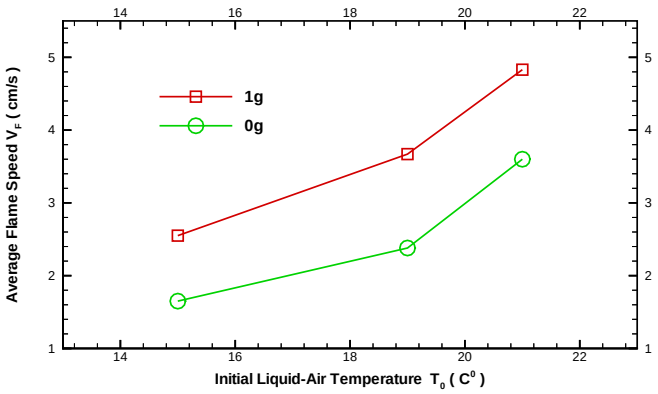

Figure 3: Average flame speed versus initial fuel-air temperature

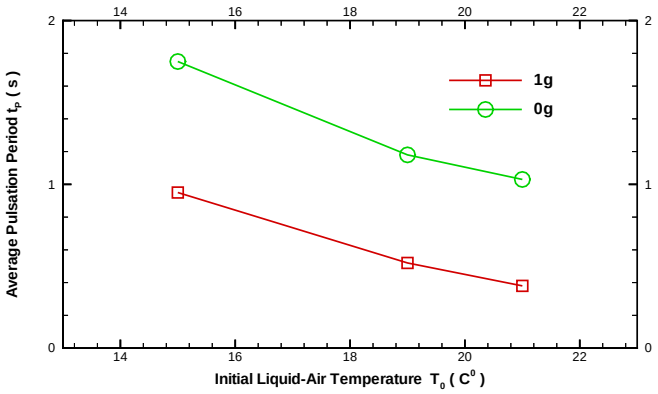

Figure 4: Average pulsation period versus initial fuel-air temperature

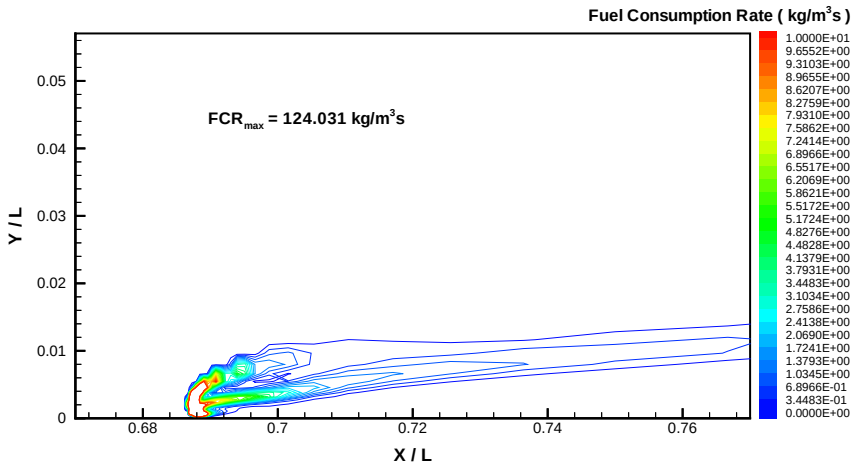

Figure 5: Contours of fuel consumption rate in the x-y symmetry plane at $z/L = 0.0$, $t = 1.63$s, Case 1A.

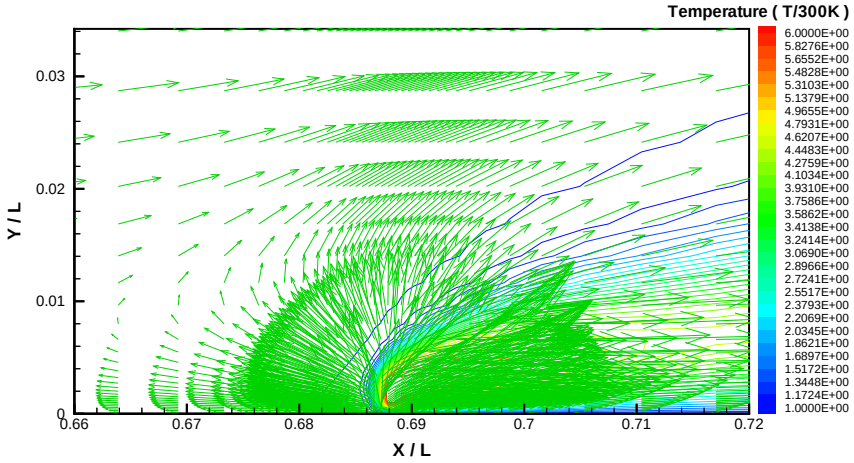

Figure 6: Contours of temperature and velocity vectors in the x-y symmetry plane at $z/L = 0.0$, $t = 1.63$s, Case 1A.

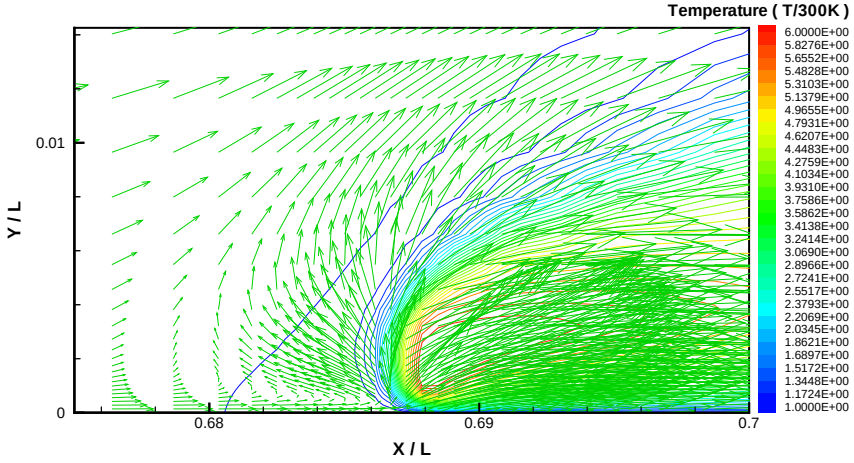

Figure 7: Contours of temperature and relative velocity vectors in the x-y symmetry plane at $z/L = 0.0$, $t = 1.63$s, Case 1A.

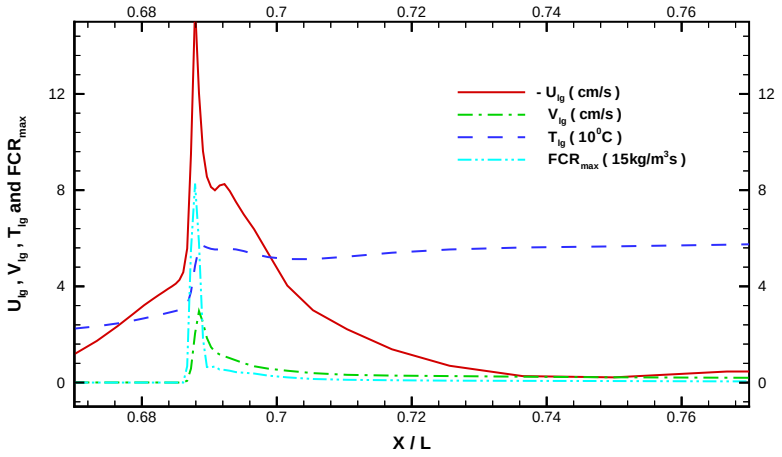

Figure 8: Flow velocity, temperature, fuel vapor vertical velocity at the fuel-air interface, and maximum fuel consumption rate at $z/L = 0.0$, $t = 1.63$s, Case 1A.

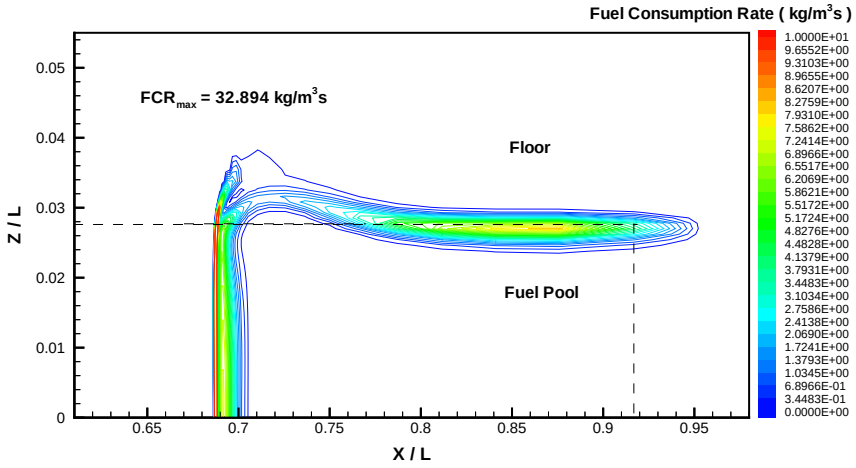

Figure 9: Contours of fuel consumption rate in the x-z plane at $y = 1$ mm, $t = 1.63$s, Case 1A.

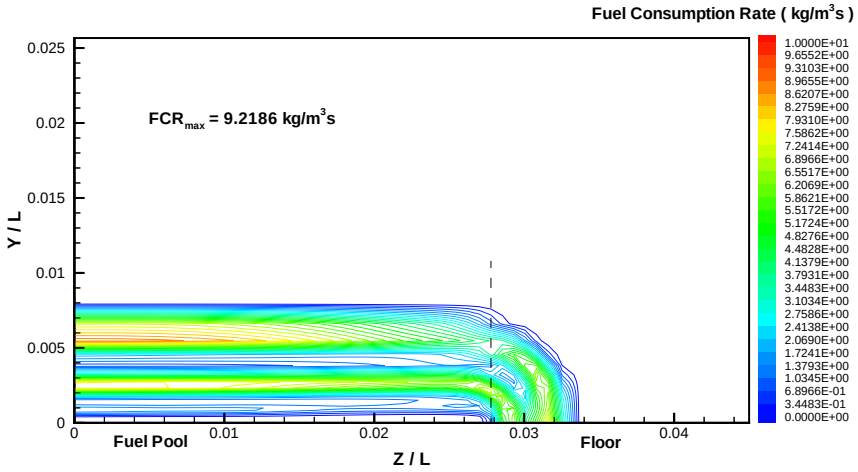

Figure 10: Contours of fuel consumption rate in the z-y plane at $x/L = 0.691$, $t = 1.63$s, Case 1A.

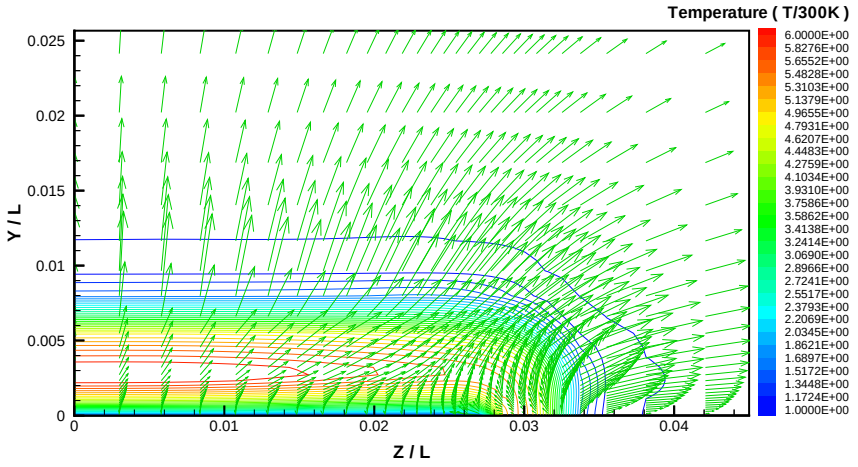

Figure 11: Velocity vector and contours of temperature in the z-y plane at $x/L = 0.691$, $t = 1.63$s, Case 1A.

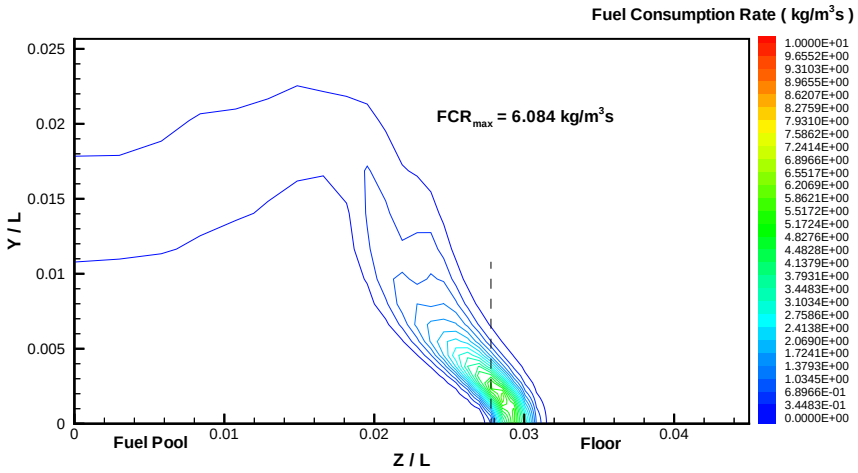

Figure 12: Contours of fuel consumption rate in the z-y plane at $x/L = 0.788$, $t = 1.63$s, Case 1A.

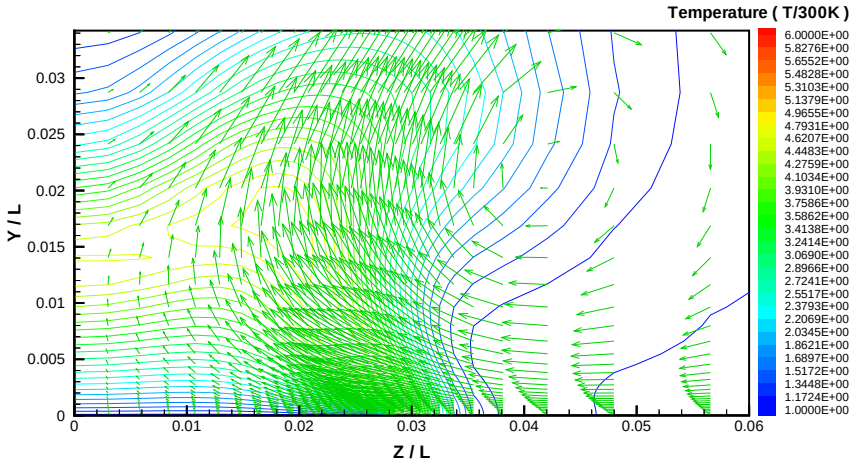

Figure 13: Velocity vector and contours of temperature in the z-y plane at $x/L = 0.788$, $t = 1.63$s, Case 1A.

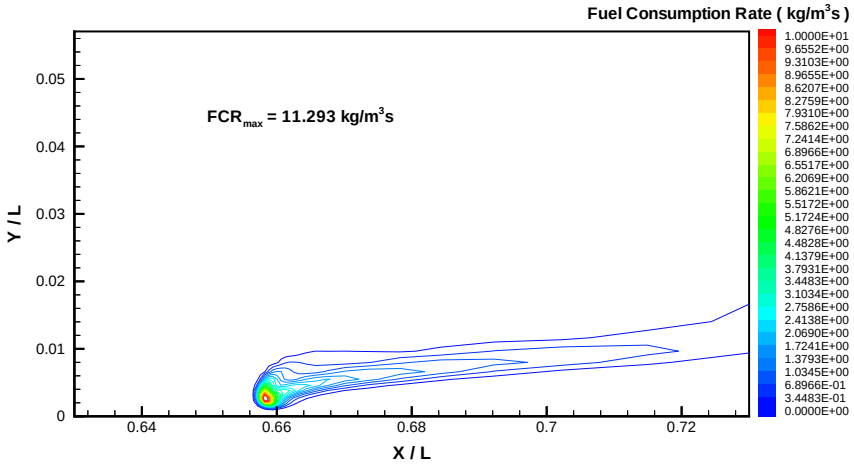

Figure 14: Contours of fuel consumption rate in the x-y symmetry plane at $z/L = 0.0$ $t = 1.87$s, Case 1A.

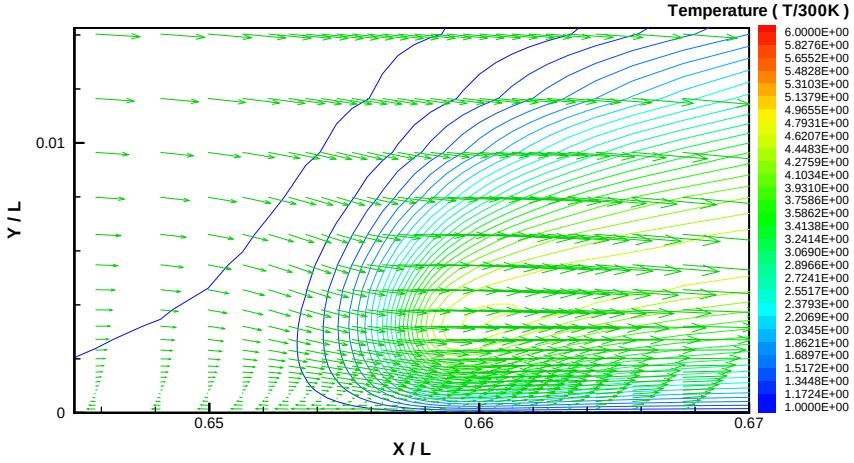

Figure 15: Relative velocity vectors and temperature contours in the x-y symmetry plane at $z/L = 0.0$ $t = 1.87$s, Case 1A.

situation at $t = 1.63$ second when the flame is moving fast, there is not a thin layer of premixed fuel-air mixture feeding into the flame near the pool surface ahead of the flame. Consequently, the combustion intensity is low. However, the clockwise vortex ahead and under the flame region draws the the fuel vapor rich mixture immediately below the flame upstream. After a certain amount of time when the fuel-air mixture is accumulated enough in front of the slow moving flame, the flame starts to propagate fast again, drawing in the pre-mixed fuel-air mixture as shown by Figure 7. The ensuing strong reaction will then deplete the pre-mixed fuel-air mixture quickly and then the above slow burning process repeats itself. The frequency of this pulsating combustion is dictated by the time needed to build up the pre-mixed fuel-air region in front of the flame when it is in the slow burning mode. This time depends on the initial fuel-air temperature, gravity level and the oxygen concentration in the air.

Figure 16 shows the top view of the flame in terms of the fuel consumption rate at $y = 1$ mm above the pool. The basic three-dimensional structure of the flame remains the same as in the previous fast burning instant. The flame still exists along the edge of the pool except that it is relatively weaker compared to that shown in Figure 9.

Case 1B. Consider the same case as Case 1A except under zero gravity. Figure 17 shows the contours of fuel consumption rate in the x-y plane in the middle of the pool at $t = 2.08$ second after ignition when the flame is in the fast moving mode. Figure 18 shows the relative velocity field and the temperature contours in the mid plane. Although the average flame speed is lower compared to the case with normal gravity, the instantaneous flame

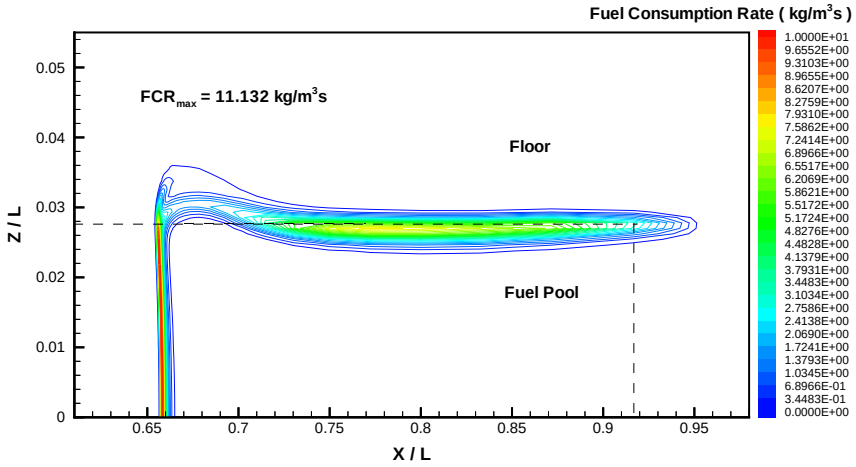

Figure 16: Contours of fuel consumption rate in the x-z plane at $y = 1$ mm, $t = 1.87$s, Case 1A.

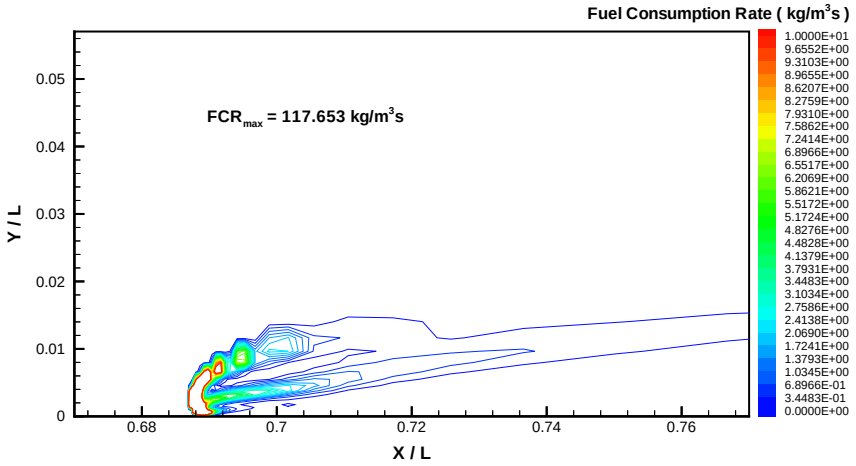

Figure 17: Contours of fuel consumption rate in the x-y plane at $z/L = 0.0$, $t = 2.08$s, Case 1B.

speed in its fast moving mode is actually faster than the flame under normal gravity in its fast moving mode. This is evidenced by the steeper slope in the time history of the flame locations shown in Figure 2. Because of this fast moving speed of the flame, the speed of the oncoming flow in the relative velocity plot, Figure 18, appears larger compared to that shown in figure 7 for the normal gravity case. The axial flow velocity at the center of the flame, however, remains close to zero. The same thin layer of flow moving into the flame exists near the surface of the fuel pool as in the normal gravity case.

Figure 19 plots distribution the flow velocity, temperature, fuel vapor vertical velocity at the fuel-air interface, and maximum fuel consumption rate through flame region. It is clear that the basic structure of the flame is the same as in the normal gravity case except that the flame is now burning at a slower rate and moving upstream at a lower speed. The temperature behind the flame is also slightly lower than in the normal gravity case.

Figure 20 shows the flame in the zero gravity case in the x-z plane at $y = 1$ mm above the pool surface. The flame still displays a similar three-dimensional curving effect and the double bifurcation at the corner of the flame front near the pool edge as in the normal gravity case. However, the flame does not continue significantly along the sides of the pool. Unlike in the case of normal gravity shown in Figures 12 and 13, cross sectional plots (not shown here) downstream of the flame front reveals very low reaction intensity at $x/L = 0.788$ and no significant streamwise vortex along the pool edge.

At time $t = 2.65$ second after ignition, the flame is in the middle of its slow motion mode as shown in Figure 2. Figure 21 shows the contours of fuel consumption rate in the x-y plane at $z/L = 0.0$. Figure 22 plots the

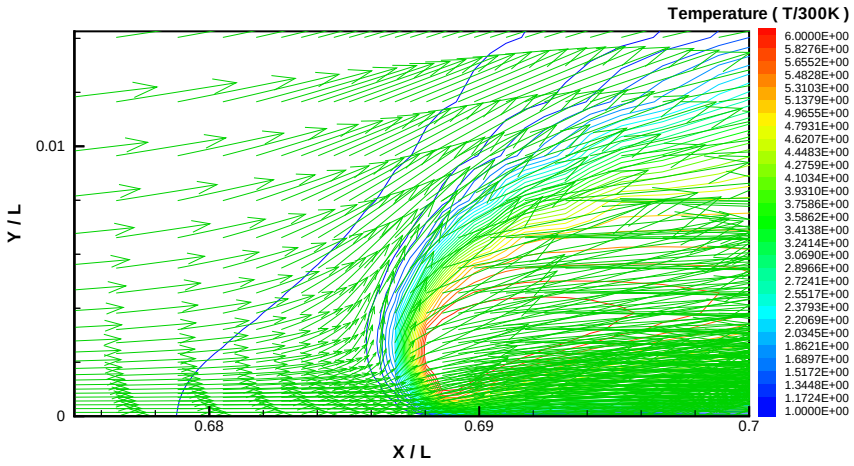

Figure 18: Relative velocity vector and contours of temperature in the x-y symmetry plane at $z/L = 0.0$, $t = 2.08$s, Case 1B.

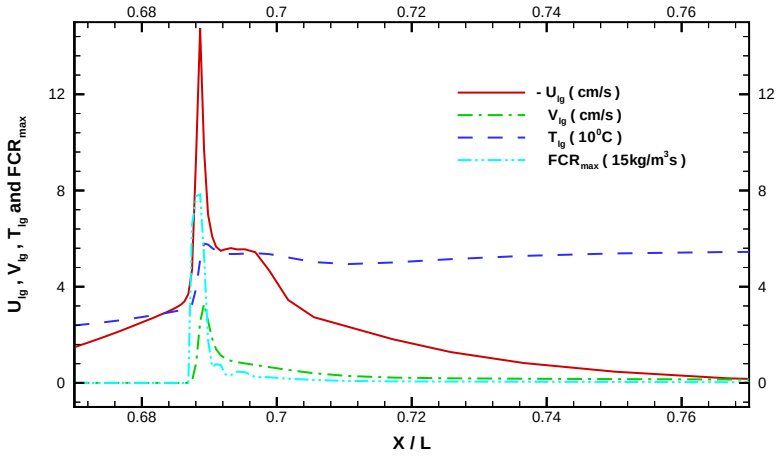

Figure 19: Flow velocity, temperature, fuel vapor vertical velocity at the fuel-air interface, and maximum fuel consumption rate (searched along y direction) versus x at $z/L = 0.0$, $t = 2.08$s, Case 1B.

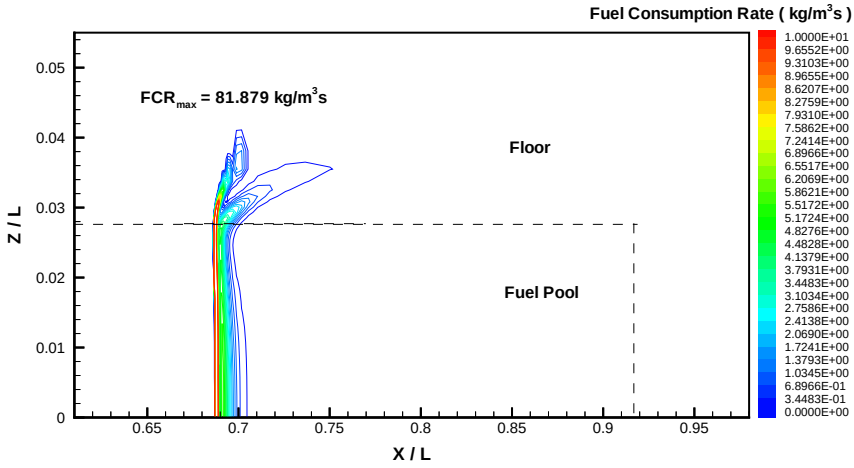

Figure 20: Contours of fuel consumption rate in the x-z plane at $y = 1$ mm, $t = 2.08$s, Case 1B.

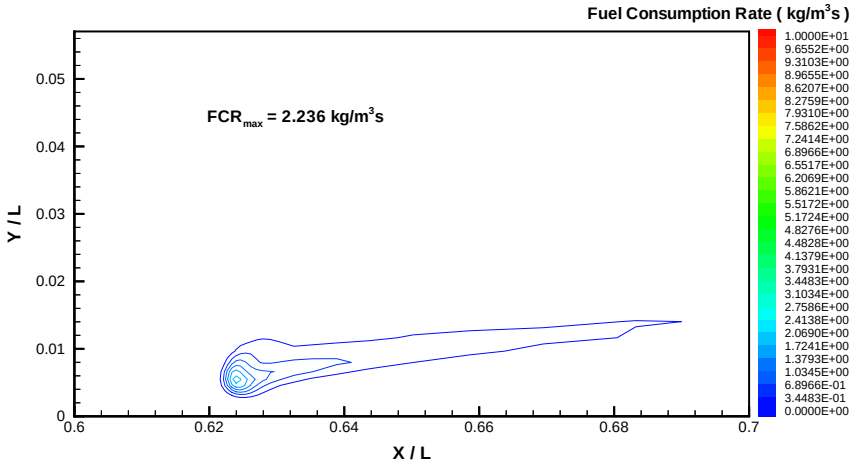

Figure 21: Contours of fuel consumption rate in the x-y plane at $z/L = 0.0$, $t = 2.65$s, Case 1B.

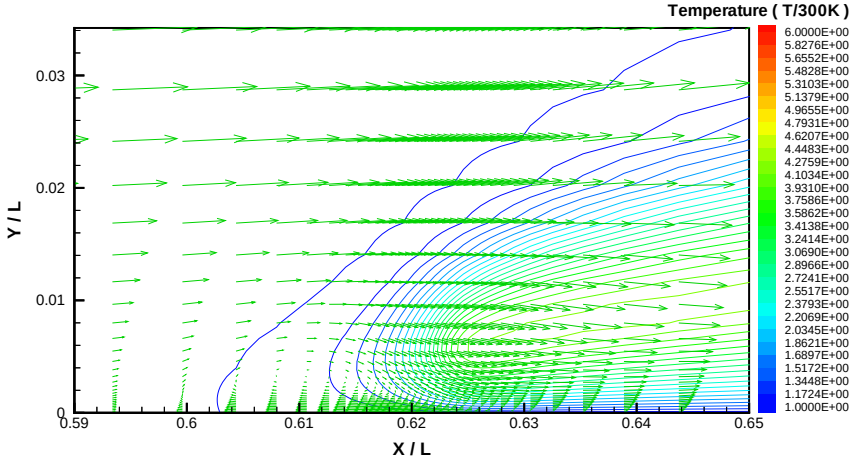

Figure 22: Relative velocity vectors and temperature contours in the x-y plane at $z/L = 0.0$, $t = 2.65$s, Case 1B.

relative velocity vectors in the same plane. As in the normal gravity case, the flow field creates a small clockwise vortex cell in front of the flame, which again helps transport the fuel-vapor rich mixture upstream from behind the flame during this slow burning period. After a sufficient amount of time when there is enough fuel-air mixture in front of the flame, the flame would start moving fast again as if in a pre-mixed region, therefore triggering another pulsating cycle. Since the flame in the zero gravity case is weaker than in the normal gravity situation due to the lack of buoyancy, it take a longer time to build up this pre-mixed fuel-air mixture in front of the flame. Consequently, the pulsating period becomes longer compared to that in the normal gravity case. Nevertheless, the basic mechanism remains the same.

6 Conclusions

A three-dimensional computational code has been developed to solve the coupled reactive flow problem of forced gas phase flow over liquid fuel. Ignition and flame spread of forced air flow above an n-propanol fuel initially below the flashpoint temperature are studied. Three-dimensional effects of the flame front near and along the edge of the pool are captured in the computation. The flame front curves backwards at the pool edge and then trails along the edge. The flame extends beyond the edge of fuel pool to be attached to the wind-tunnel wall. Thermal expansion and buoyancy effects creates a streamwise vortex near the two edges of the liquid pool. Flame pulsation is found at both normal gravity and zero gravity for all three cases of initial fuel-air temperature with 30 cm/s opposed flow.

Computations show that the mechanism of flame pulsation is due to the formation of a gas-phase recirculation zone resulting from the balance of the forced flow, thermal expansion, buoyancy if it exists, and thermo-capillary surface tension in the liquid fuel. This recirculation transports fuel-vapor upstream from below and behind an initially slow moving flame until it builds a sizable pre-mixed fuel-air mixture in front of the flame. The flame will then move fast and deplete the pre-mixed zone before it enters the slow moving phase again. pulsating spread of the flame. The pulsation frequency depends on the initial fuel-air temperature and gravity levels. Higher initial fuel-air temperature gives a higher frequency. Microgravity, on the other hand, reduces the pulsation frequency.

There is qualitative agreement between these results and the prior two-dimensional results [2]. Important differences between this configuration (with three-dimensional side effects and closed air channel) versus the previous study (with no side effects and open environment) do exist so that some differences in the global features can be expected. These preliminary results demonstrate the usefulness of the three-dimensional computations. Further studies will include more detailed simulation of the propagation of the flame over the whole pool surface and also variation of parameters such as forced flow speed, initial temperature, liquid pool width and depth.

Acknowledgments

This research was conducted in support of NASA Grant No. NAG3-2024 under the technical monitoring of Dr. Howard Ross. Computer time was provided by the San Diego Supercomputer Center, the NASA Center for Computational Sciences, and the UCI Network and Academic Computing Services.

References

[1] Schiller, D. N., Ross, H. D., and Sirignano, W. A., "Computational Analysis of Flame Spread Over Alcohol Pools," *Combustion Science and Technology*, Vol. 118, No. 4-6, May 1996, pp. 205–258.

[2] Schiller, D. N. and Sirignano, W. A., "Opposed-Flow Flame Spread Across n-Propanol Pools," *Proceedings of the Twenty-Sixth International Symposium on Combustion*, 1996, pp. 1319–1325.

[3] Ross, H. D. and Miller, F. J., "Flame Spread Across Liquid Pools with Very Low-Speed Opposed or Concurrent Airflow," *Proceedings of the Twenty-Seventh International Symposium on Combustion*, 1998, pp. 2723–2729.

[4] Miller, F. J. and Ross, H. D., "Smoke Visualization of the Gas-Phase Flow During Flame Spread Across a Liquid Pool," *Proceedings of the Twenty-Seventh International Symposium on Combustion*, 1998, pp. 2715–2722.

[5] Kim, I., Schiller, D. N., and Sirignano, W. A., "Axisymmetric Flame Spread Across Propanol Pools in Normal and Zero Gravities," *Combustion Science and Technology*, Vol. 139, No. 1-6, 1999, pp. 249.

[6] Patankar, S. V., *Numerical Heat Transfer and Fluid Flow*, Hemisphere, New York, 1980.